MICRO- AND MACRO-MECHANICAL APPROACHES FOR MODELLING OF POLYETHYLENE MATERIAL FOR PIPES

J.A. Alvarado-Contreras[1,3], H. Liu[1], M.A. Polak[1,*] and A. Penlidis[2]
[1]*Department of Civil Engineering, University of Waterloo, Waterloo, ON, Canada*
[2]*Department of Chemical Engineering, University of Waterloo, Waterloo, ON, Canada*
[3]*School of Mechanical Engineering, University of the Andes, Mérida, Venezuela*

Abstract

Two different approaches for modelling the mechanical behaviour of polyethylene materials are presented. In the first one, the emphasis is on the relationships between molecular features and mechanical properties. In the proposed model, the material is analyzed from a microscopic viewpoint and considered as an aggregate of crystals. The constitutive equation is expressed in a viscoplastic framework considering degradation at large deformations. For the second approach, the material response is considered to be nonlinear viscoelastic. A phenomenological approach is adopted, and attention is given on the formulation of a model that can be implemented for structural analysis of components such as pipes. In this part of the study, numerical and experimental data of creep for a medium-density polyethylene pipe material are presented. The efficacy of the micro- and macro-mechanical approaches is confirmed by experimental results.

1. Introduction

Polyethylene material has been widely used since the early 1940s. Its low cost, lightness, and chemical stability have favoured its popularity to substitute other materials in water, gas, and sewage disposal pipelines. During installation and utilization, pipes are typically subjected to complex loads and loading paths. This has motivated the interest, first, in understanding the relationships between molecular structure and end-use mechanical performance, and then, in improving the material properties. Many studies have concentrated on experimental and theoretical aspects of nonlinear history-dependent behaviour and on the deformation mechanisms at large deformations. The present work consists of two parts. The first one deals with the modelling of the mechanical response of polyethylene material from a microstructural viewpoint. The second part presents the macroscale approach to modelling the nonlinear behaviour of polyethylene based on responses obtained experimentally.

2. Structure of Polyethylene

Polymeric materials are made of macromolecules and appear in a variety of products. These macromolecules are long chains of thousands of repeating units, which give polymers many of their useful properties. In polyethylene, molecules are basically long chains of carbon and hydrogen atoms. The smallest unit (monomer) is ethylene (C_2H_4), whereas a typical polyethylene molecule contains from approximately 900 to 215,000 of these units. It has been shown that polyethylene possesses a structure with spherulitic morphology, as illustrated in Figure 1. Within this structure, molecules are capable of adopting two distinct arrangements, the amorphous and crystalline phases. Amorphous polyethylene is characterized by those segments where molecules have, on average, no favoured directions. On the order hand, crystalline polyethylene corresponds to segments of highly ordered molecules embedded within the amorphous phase. Polyethylene crystals form

* Corresponding author: M.A. Polak, E-mail: *polak@uwaterloo.ca*

M. Pandey et al. (eds), Advances in Engineering Structures, Mechanics & Construction, 449–458.

by folding the molecules alternately up and down and by arranging the straight segments between folds into a periodic array. The thickness of polyethylene crystals ranges from 50 to 250 Å (Å=10^{-10} m), and the lateral dimensions range from 1 to 50×10^{-6} m. Only about 40 monomeric units are included in each of the straight segments between folds (Lin & Argon, 1994). The structure of a crystal is of the orthorhombic crystal class, as illustrated in Figure 1. The parameters a, b, and c are the lattice parameters, where the c-axis is parallel to the molecules.

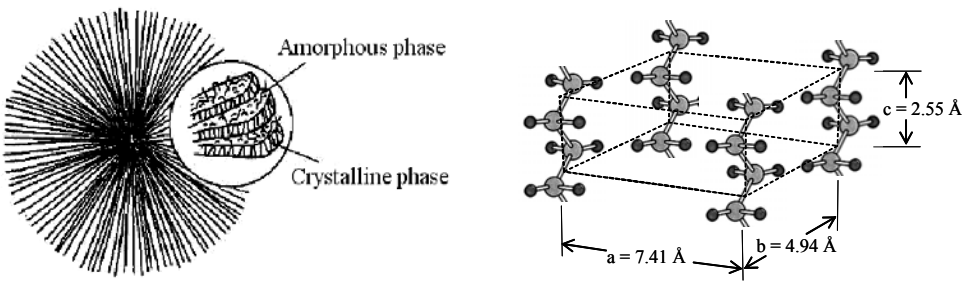

Figure 1. Schematic illustration of a polyethylene spherulitic structure and a crystal.

According to the American Society for Testing and Materials, polyethylene can be classified into four groups. Low-density polyethylene (LDPE) has a density ranging from 0.91 to 0.93 g/cm^3 and is predominantly amorphous. Medium-density polyethylene (MDPE) typically has average densities from 0.93 to 0.94 g/cm^3. High-density polyethylene (HDPE) has a density above 0.94 g/cm^3 with only a few branched chains. As a result, these molecules align into more compact arrangements with up to 90% crystalline regions. Linear low-density polyethylene (LLDPE) has longer and more branches than HDPE. Consequently, it has a higher density than LDPE but still a linear structure like HDPE.

3. Constitutive Micro-modelling

Although microstructure and mechanical properties of polymers have been the subject of many studies, it is only during the last two decades or so that deformation mechanisms have been properly described. The earlier models aid in the interpretation of structural observations under different loading conditions; however, they cannot predict the microstructural damage caused by deformation. The proposed model is expressed in the framework of viscoplasticity coupled with degradation at large deformations. This involves the concepts of damage mechanics considering the original microstructure, the particular irreversible rearrangements, and the deformation mechanisms. As mentioned above, molecules in polyethylene materials can adopt two basic arrangements. Nevertheless, to simplify the complex microstructure, the model regards the material exclusively as crystalline; the amorphous phase is ignored. Thus, a three-dimensional aggregate of randomly oriented and perfectly bonded crystals is used to describe the behaviour. In an aggregate, crystals are much larger than molecules, but smaller than material points. Initially, the material is assumed to be micro- and macro-scopically homogeneous.

The theoretical formulation of the micromechanical model has been presented in detail in Alvarado-Contreras et al. (2005). Consequently, we limit ourselves to a brief description of the most important features of the model, as summarized in Table 1. The model solves the stress-strain problems in two stages, one for the microscopic problem (local problem) and the other for coupling the micro- and macro-scopic problems (global problem).

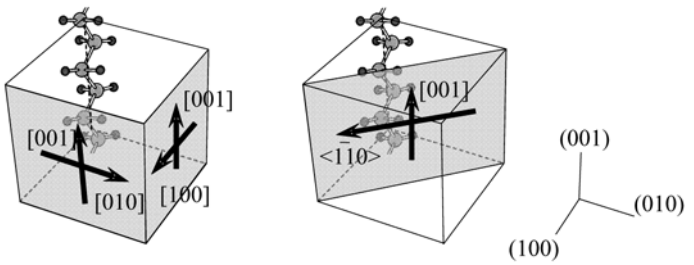

Figure 2. Slip systems in polyethylene crystals.

At the local problem, deformation mechanisms in single crystals are considered. These mechanisms are based on the theory of shear slip on crystallographic planes (Asaro & Rice, 1977). The material is initially isotropic and homogeneous, and the elastic deformations are ignored (realistic for large deformation analyses). The slip plane normal $\mathbf{n}^{\alpha}$ and slip direction $\mathbf{s}^{\alpha}$ define the slip systems (Figure 2). The second-order tensors $\mathbf{R}^{\alpha}$ and $\mathbf{A}^{\alpha}$ represent symmetric and skew-symmetric orientation tensors associated with the slip systems, as shown in Eq. 1. The deformation rate $\mathbf{D}$ and plastic spin $\mathbf{W}^{p}$ are consequences of the shear rates $\dot{\gamma}^{\alpha}$ on all slip systems, as indicated in Eq. 2 (Asaro, 1979). The constitutive equation connecting the microscopic deviatoric stress $\mathbf{S}$ and deformation rate $\mathbf{D}$ is expressed in Eq. 3. Here, the fourth-order compliance tensor M, based on a power-law model for the shear rates, is characterized by the inverse of the rate sensitivity n, the reference shear rate $\dot{\gamma}_0$, and the current critical shear strengths g^{α} (Eq. 4). Furthermore, Ω^{α} is a simple scalar damage variable associated with the atomic debonds of the slip planes, and it evolves according to the evolution law given in Eq. 5, where $\dot{\Omega}_0$ and m are the reference damage rate and rate exponent. Noting that damage and hardening processes may be considered independent of each other (Leimatre & Chaboche, 1994), the rate of hardening of a slip system evolves according to Eq. 6, where h_0 and c characterize the slip system hardening and saturation strength, respectively. To estimate the crystal orientation evolution, the local spin $\mathbf{W}$ is calculated as the sum of the rigid-body spin $\mathbf{W}^{*}$ and the plastic spin $\mathbf{W}^{p}$, where the plastic component is affected by an empirical release parameter Ψ which is a function of the material parameter ζ and slip system damage Ω^{α}, as specified in Eq. 7.

In general, microstructure and its changes are non-deterministic. The same is true for the fluctuations in stresses and strains. Thus, for the global problem, the macroscopic mechanical behaviour is calculated as a volume average of the corresponding crystal responses. First, let $\overline{\mathbf{D}}$ and $\overline{\mathbf{W}}$ be, respectively, the macroscopic deformation rate and spin applied to the crystal aggregate at some material point. The partition of the deformation rate among the crystals is calculated through Eq. 8, where P is a local fourth-order projection tensor that considers the inextensibility of the crystal molecules, and $\overline{\mathrm{P}}^{-1}$ represents the inverse of its volume average (Parks & Ahzi, 1990). Conversely, crystal spins, having only three independent components, simply equal the global spin, as in Eq. 9. Based on the above steps, the global response is estimated by averaging the stresses in all crystals. Then, if the homogenized reduced stress $\overline{\mathbf{S}}$ satisfies the boundary conditions to adequate tolerance, the solution is accepted. Otherwise, corrections based on the successive substitution scheme are performed, and the procedure is repeated using $\overline{\mathbf{S}}$ as a new trial stress. Once an estimate of $\overline{\mathbf{S}}$ has been found, it can be related to the global deformation rate $\overline{\mathbf{D}}$ throughout the relationship given in Eq. 10, where $\overline{\mathrm{M}}$ is the global average compliance tensor.

Table 1. Summary of the micro-mechanical model.

Local problem		
[1]	$\mathbf{R}^{\alpha} = \frac{1}{2}(\mathbf{n}^{\alpha} \otimes \mathbf{s}^{\alpha} + \mathbf{s}^{\alpha} \otimes \mathbf{n}^{\alpha})$ and $\mathbf{A}^{\alpha} = \frac{1}{2}(\mathbf{n}^{\alpha} \otimes \mathbf{s}^{\alpha} - \mathbf{s}^{\alpha} \otimes \mathbf{n}^{\alpha})$	Schmid tensors
[2]	$\mathbf{D} = \sum_{\alpha=1}^{8} \dot{\gamma}^{\alpha} \mathbf{R}^{\alpha}$ and $\mathbf{W}^{p} = \sum_{\alpha=1}^{8} \dot{\gamma}^{\alpha} \mathbf{A}^{\alpha}$	Deformation rate and plastic spin
[3]	$\mathbf{D} = \mathrm{M} : \mathbf{S}$	Local constitutive equation
[4]	$\mathrm{M} = \dot{\gamma}_0 \sum_{\alpha=1}^{8} \left(\frac{1}{(1-\Omega^{\alpha}) g^{\alpha}} \right)^{n} \left| \mathbf{S} : \mathbf{R}^{\alpha} \right|^{n-1} \mathbf{R}^{\alpha} \otimes \mathbf{R}^{\alpha}$	Compliance tensor
[5]	$\frac{d\Omega^{\alpha}}{d\tau^{\alpha}} = \dot{\Omega}_0 \left| \frac{\mathbf{S} : \mathbf{R}^{\alpha}}{(1-\Omega^{\alpha}) g^{\alpha}} \right|^{m}$	Damage evolution law
[6]	$\frac{d\dot{g}^{\alpha}}{d\dot{\gamma}^{\alpha}} = h_0 \mathrm{sech}^2 \left(\frac{h_0}{c} \bar{\gamma} \right)$, where $\bar{\gamma} = \int_0^t \sum_{\alpha=1}^{8} \dot{\gamma}^{\alpha} dt$	Hardening evolution law
[7]	$\mathbf{W} = \mathbf{W}^{*} + \Psi \mathbf{W}^{p}$, where $\Psi = \tanh(\frac{1}{8} \zeta \sum_{\alpha=1}^{8} \Omega^{\alpha})$	Local spin
Global problem		
[8]	$\mathbf{D} = \mathrm{P} : \overline{\mathrm{P}}^{-1} : \overline{\mathbf{D}}$	Deformation rate partition
[9]	$\mathbf{W} = \overline{\mathbf{W}}$	Spin partition
[10]	$\overline{\mathbf{D}} = \overline{\mathrm{M}} : \overline{\mathbf{S}}$	Global constitutive equation

4. Numerical Results (Micro-mechanical Approach)

This section shows the capability of the model to represent the mechanical behaviour of high-density polyethylene based only on its crystalline microstructure. Calculations are carried out for an initially isotropic aggregate of 100 crystals in uniaxial tension. In the simulations, the deformation rate is prescribed, and the crystal stresses and orientation changes are determined. From them, the macroscopic stress state is calculated. Considering axisymmetric boundary conditions, a constant macroscopic strain rate of 10^{-3}/s and null macroscopic spin are applied. For each crystal, all eight slip systems are active and the initial resolved shear strengths are known, as listed in Table 2 (Parks & Ahzi, 1990). The material parameters are fitted from two tensile tests obtained from the literature (Hillmansen et al., 2000; G'Sell et al., 2002).

Figure 3 shows the normalized equivalent macroscopic stress $(\bar{\sigma}/\tau_0)$ versus the equivalent strain. The stress values are normalized using a τ_0 = 7.2MPa. This figure shows most of the features of the experimental responses are reproduced up to certain deformation values. The strengthening observed in the experimental tests is accounted for by adjusting the saturation strength c while the other parameters (see Table 3) remain unchanged. Two values for the saturation strength c in Eq. 6 were used, c = 0.75 and 5. As shown, the higher the c-value, the higher the stress rate (represented by the curve slope for a given equivalent deformation). Comparing, the calculated responses are stiffer than those observed in real polyethylene. This earlier strengthening is obvious at large deformations. As shown in Figure 3, an upturn in the stress-strain curve occurs beyond a strain of 1.3 for c = 0.75. This

illustrates the importance of both the crystal lattice spin and the amorphous phase for large deformations; this last feature is ignored in the current formulation.

Figure 4 shows the evolution of the damage average for the eight slip systems for the case with c = 0.75. The solid and broken lines represent the damage evolution for the transverse and chain slip systems, respectively. The profiles depicted in the figure indicate that the largest damage values occur on the $(100)[001]$, $(110)[1\bar{1}0]$, and $(1\bar{1}0)[001]$ slip systems. All slip systems show three damage stages; decreasing, constant, and increasing. Thus, the model represents both the variations of damage gradients for the different slip systems as material is drawn as well as the sharp gradients near failure.

Table 2. Resolved shear strengths.

Slip-system	g^{α} [MPa]
(100) [001]	7.2
(010) [001]	7.2
$(110)\langle 001\rangle$	7.2
(100) [010]	7.92
(010) [100]	12.96
$\{110\}\langle 1\bar{1}0\rangle$	12.96

Table 3. Material parameters for the simulations.

n	$\dot{\gamma}_0$ [/s]	m	$\dot{\Omega}_0$	h_0 [MPa]	ζ
5	0.001	2	0.1	5.0	40.0

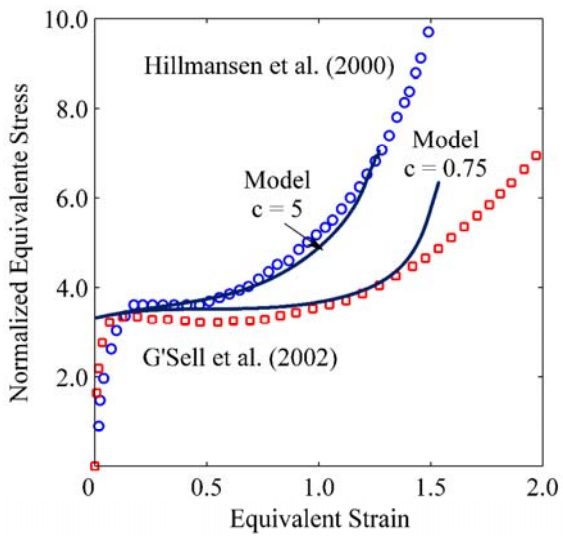

Figure 3. Normalized equivalent stress $(\overline{\sigma}/\tau_0)$ as a function of the equivalent strain for the two materials analyzed; $\overline{\sigma} = \sqrt{\frac{3}{2}\overline{\mathbf{S}} : \overline{\mathbf{S}}}$.

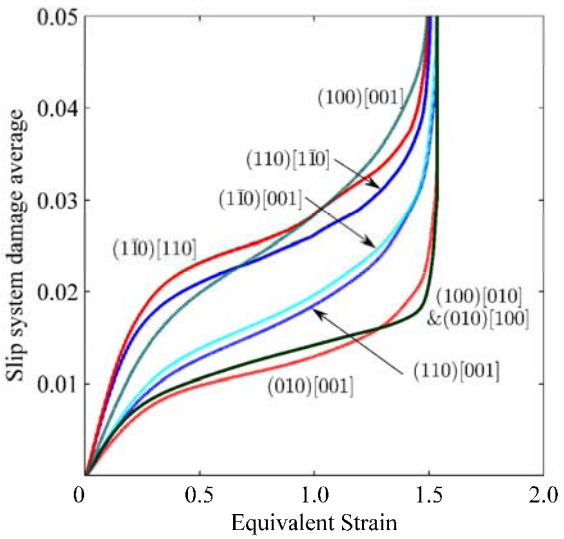

Figure 4. Evolution of damage average for the slip systems, taking c = 0.75.

5. Macro-mechanical Creep Response of Polyethylene

In viscoelasticity, the constitutive relationships are time dependent. Creep, time-relaxation, and loading rate effects are typical time-dependent responses. Creep tests are convenient for material testing and characterization. During a creep test, strain grows with time under a constant stress. The material deformation history can be described by a compliance (strain divided by stress)-time curve.

Creep tests on two high-density polyethylene (HDPE) materials were done in a previous study, and nonlinear viscoelastic models were generated for them (Liu & Polak, 2005). The models perform well in simulating creep behaviour at stresses below 10 MPa, where strains do not show drastic changes within the test durations (24 hours).

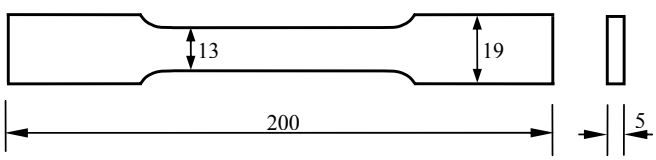

Figure 5. Material creep test specimen (units in mm).

In this study, further tests are presented for a medium-density polyethylene (MDPE) material. Tensile test specimens are cut off from a MDPE pipe, as shown in Figure 5. Creep test results for the MDPE samples are shown in Figure 6. During the test, load is applied by dead weights through a lever arm. Due to the small deformations, the (engineering) stress is assumed to be constant. A clip-on strain gauge with a data acquisition system is used to record the deformation history of the specimens. Displacements between the knife edges of the strain gauge are recorded, and the displacement-time history is converted to engineering strain-time history by dividing each displacement by the initial knife edges distance. The tests are carried out at room temperature (~22°C) for 24 hours. Figure 6(a) shows the creep strain-time curves from the tests on the MDPE pipe materials. The compliance curves at different stresses indicate strong viscoelastic nonlinearity, as shown in Figure 6(b).

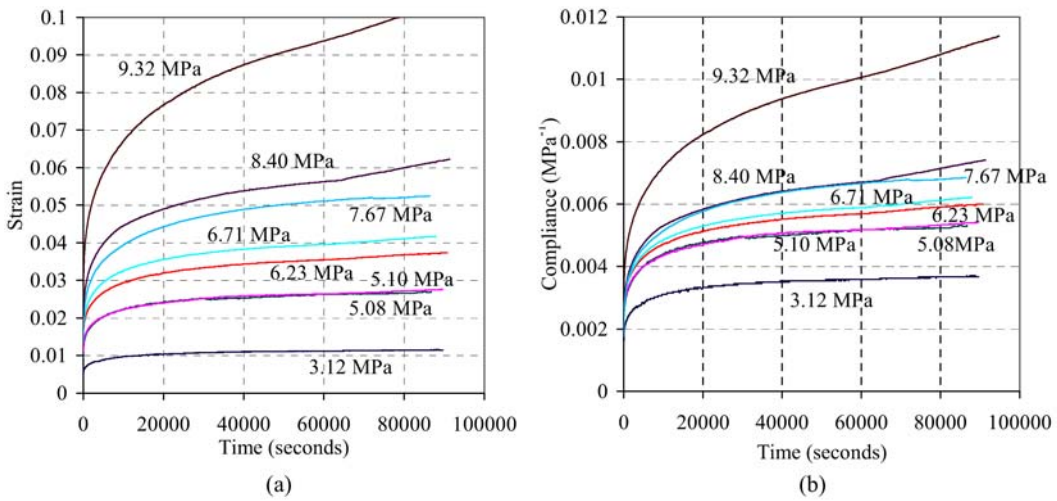

Figure 6. Creep tests for MDPE. (a) Strain-Time; (b) Compliance-Time.

6. Nonlinear Viscoelastic Modelling

Macro-modelling of polyethylene does not separate the crystalline and amorphous phase behaviour but describes the overall material behaviour in bulk. A nonlinear viscoelastic model is generated by adopting a linear interpolation approach to include stress influence on the material parameters. These parameters are taken to be piecewise linear functions instead of being prescribed functions. The model is presented as a matrix of material constants corresponding to the selected stresses. The parameters corresponding to stress levels between the stresses used for defining the model are found from a linear interpolation.

The proposed model is formulated from a multiple Kelvin element model, shown in Figure 7. The number of Kelvin elements for a specific material is determined in the calibration process. This makes the model more adaptable to material variations.

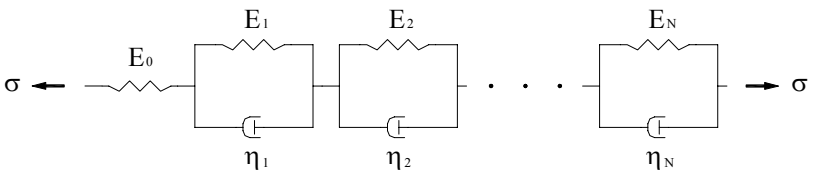

Figure 7. Multiple Kelvin element viscoelastic solid.

The constitutive equation of the nonlinear model is given by:

$$[11] \qquad \varepsilon(t) = \int_0^t \left\{ \frac{1}{E_0(\sigma)} + \sum_{i=1}^{N} \frac{1}{E_i(\sigma)} \left[1 - \exp\left(-\frac{t-\tau}{\tau_i} \right) \right] \right\} \dot{\sigma}(\tau) d\tau$$

where E_0 and E_i are functions of stress, and $\tau_i = \eta_i / E_i$, known as relaxation times, remain constant. η_i are the Kelvin dashpot viscosities. The creep function is given by:

$$[12] \qquad \psi(t) = \frac{1}{E_0(\sigma)} + \sum_{i=1}^{N} \frac{1}{E_i(\sigma)} \left[1 - \exp\left(-\frac{t}{\tau_i} \right) \right]$$

Then, the strain response under a constant stress σ_i becomes:

$$[13] \qquad \varepsilon(t) = \sigma_i \left\{ \frac{1}{E_0(\sigma_i)} + \sum_{i=1}^{N} \frac{1}{E_i(\sigma_i)} \left[1 - \exp\left(-\frac{t}{\tau_i} \right) \right] \right\}$$

For a constant σ_i, the material parameters E_0 and E_i are calibrated from a given test and reduced to constants. For the development of the proposed model, several creep tests are performed at different stress levels. A linear least-squares fitting is used in the parameter calibration at each stress, and the number of Kelvin elements N is automatically chosen by the fitting criterion. A series of constant $E_0(\sigma_i)$ and $E_i(\sigma_i)$ values are generated corresponding to the creep stresses. Thus, the model can be presented as a table of E_0 and E_i values, as listed in Table 4.

In order to define the material behaviour at an arbitrary stress, the parameters are linearly interpolated from the parameters corresponding to stresses below and above the given value. Thus, E_0 and E_i are modelled as linear piecewise functions of stress. For modelling purposes, the instantaneous modulus $E_0(\sigma_i)$ and the coefficients of the exponential terms $x_i(\sigma_i) = 1/E_i(\sigma_i)$ (instead of $E_i(\sigma_i)$) are linearly interpolated for an arbitrary stress, σ. The interpolations are given by the following equations:

$$[14] \qquad E_0(\sigma) = E_0(\sigma_m) + \frac{\sigma - \sigma_m}{\sigma_n - \sigma_m} \left[E_0(\sigma_n) - E_0(\sigma_m) \right]$$

$$[15] \qquad x_i(\sigma) = x_i(\sigma_m) + \frac{\sigma - \sigma_m}{\sigma_n - \sigma_m} \left[x_i(\sigma_n) - x_i(\sigma_m) \right]$$

where σ_m and σ_n are the bounding stresses that define the interval in which σ is located. When the number of Kelvin elements is not equal for all the stress levels used to define the model, a zero value for the absent coefficients x_i can be used.

For numerical implementation, Eq. 11 can be discretized as:

$$[16] \qquad \varepsilon_k = \sum_{j=1}^{k} \left\{ \frac{1}{E_0} + \sum_{i=1}^{n} \frac{1}{E_i} \left[1 - \exp\left(-\frac{t_k - t_{j-1}}{\tau_i} \right) \right] \right\} (\sigma_j - \sigma_{j-1})$$

where t_j and t_k are times at discrete steps, and σ_j and ε_k are the corresponding stress and strain.

7. Numerical Results (Macro-mechanical Approach)

Five creep tests on the MDPE pipe material were used to develop the model, as in Table 4. The parameters of the nonlinear viscoelastic model (Eq. 11) are given in Table 4. Figures 8 and 9 compare experimental and simulated data. It is shown that the simulated strain data fit well. At stress levels other than those used for model development, the simulations match the experimental results as well, except when close to the highest stress (9.32 MPa) where the strain curve changes drastically and digresses from the main group strain (see Figure 9). Similar results have been found for HDPE materials at stresses higher than 10 MPa, as shown by Liu and Polak (2005).

Table 4. Nonlinear viscoelastic model for MDPE. Kelvin elements = 3.

		$\tau_1 = 500$	$\tau_2 = 10000$	$\tau_3 = 200000$
Stress (MPa)	E_0 (MPa)	E_1	E_2	E_3
3.12	640	1137.4169	1067.2127	1168.6089
5.10	470	804.3798	718.0750	588.7810
6.23	420	813.3631	668.5170	422.0754
8.40	410	690.8382	572.2448	224.6822

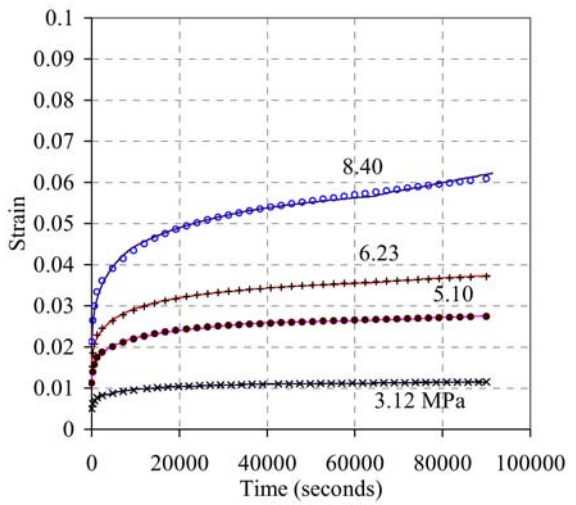

Figure 8. Creep tests vs. model simulations at modelling stresses.

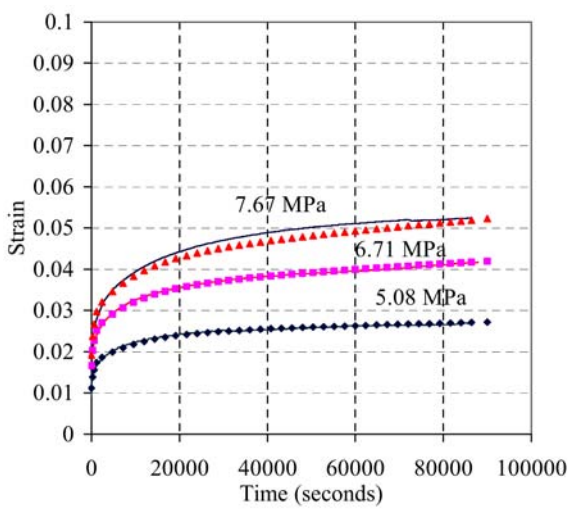

Figure 9. Creep tests vs. model simulations at verification stresses.

8. Conclusions

Two different approaches to study the mechanical behaviour of medium- and high-density polyethylene subjected to uniaxial tension are presented. From the results, the following conclusions can be drawn: 1) The described theories offer practical avenues of obtaining accurate representations of the behaviour of polyethylene from both the micro- and macro-scopic viewpoints; 2) For the microscopic approach, it is possible to couple the various deformation mechanisms and degradation processes taking place at the crystal level; 3) Material parameters are easily defined from experimental tensile tests; 4) The numerical stress-strain responses agree, up to certain deformations, with the experimental ones obtained by Hillmansen et al. (2000) and G'Sell et al. (2002); 5) For the macroscopic approach, the model simulates well the creep behaviour of medium- and high-density polyethylene; 6) The material parameters are obtained from creep tests directly on pipe material; 7) The model represents well the strong nonlinear viscoelasticity observed experimentally at intermediate stress levels; and 8) Both approaches could be applied to model other polymeric materials.

References

Alvarado-Contreras, J. A., Polak, M. A., and Penlidis, A. 2005. Damage modelling of polyethylene. *Proceedings of the 33d Annual General Conference of the Canadian Society for Civil Engineering*, Toronto, GC-185: 1-10.

Asaro, R. J. 1979. Geometrical effects in the inhomogeneous deformation of ductile single crystals. *Acta Metallurgica*, 27: 445-453.

Asaro, R. J. and Rice, J. R. 1977. Strain localization in ductile single crystals. *Journal of the Mechanics and Physics of Solids*, 25: 309-338.

G'Sell, C., Dahoun, A., Hiver, J. M., and Addiego, F. 2002. Compétition des mécanismes de cisaillement plastique et d'endommagement dans les polymers solides en traction uniaxiale, *Matériaux*, 1-5.

Hillmansen, S., Hobeika, S., Haward, R. N., and Leevers, P. S. 2000. The effect of strain rate, temperature, and molecular mass on the tensile deformation of polyethylene. *Polymer Engineering and Science*, 40: 481-489.

Lemaitre, J. and Chaboche, J. L. 1994. *Mechanics of Solid Materials*. Cambridge: Cambridge University Press.

Lin, L. and Argon, A. S. 1994. Review: Structure and plastic deformation of polyethylene. *Journal of Materials Science*, 29: 294-323.

Liu, H. and Polak, M. A. 2005. Nonlinear viscoelastic modelling of creep of polyethylene. *Proceedings of the 33d Annual General Conference of the Canadian Society for Civil Engineering*, Toronto, GC-140: 1-10.

Parks, D. M. and Ahzi, S. 1990. Polycrystalline plastic deformation and texture evolution for crystals lacking five independent slip systems. *Journal of the Mechanics and Physic of Solids*, 38: 701-724.